The Plant Cell, Vol. 27: 3213–3227, November 2015, www.plantcell.org

Light-Harvesting Complex Stress-Related Proteins Catalyze Excess Energy Dissipation in Both Photosystems of *Physcomitrella patens*

Alberta Pinnola,[a] Stefano Cazzaniga,[a] Alessandro Alboresi,[a,1] Reinat Nevo,[b] Smadar Levin-Zaidman,[c] Ziv Reich,[b] and Roberto Bassi[a,2]

[a] Department of Biotechnology, University of Verona, 37134 Verona, Italy
[b] Department of Biological Chemistry, Weizmann Institute of Science, Rehovot 76100, Israel
[c] Electron Microscopy Unit, Weizmann Institute of Science, Rehovot 76100, Israel

ORCID IDs: 0000-0001-8373-7638 (A.P.); 0000-0003-4818-7778 (A.A.); 0000-0002-4140-8446 (R.B.)

Two LHC-like proteins, Photosystem II Subunit S (PSBS) and Light-Harvesting Complex Stress-Related (LHCSR), are essential for triggering excess energy dissipation in chloroplasts of vascular plants and green algae, respectively. The mechanism of quenching was studied in *Physcomitrella patens*, an early divergent streptophyta (including green algae and land plants) in which both proteins are active. PSBS was localized in grana together with photosystem II (PSII), but LHCSR was located mainly in stroma-exposed membranes together with photosystem I (PSI), and its distribution did not change upon high-light treatment. The quenched conformation can be preserved by rapidly freezing the high-light-treated tissues in liquid nitrogen. When using green fluorescent protein as an internal standard, 77K fluorescence emission spectra on isolated chloroplasts allowed for independent assessment of PSI and PSII fluorescence yield. Results showed that both photosystems underwent quenching upon high-light treatment in the wild type in contrast to mutants depleted of LHCSR, which lacked PSI quenching. Due to the contribution of LHCII, *P. patens* had a PSI antenna size twice as large with respect to higher plants. Thus, LHCII, which is highly abundant in stroma membranes, appears to be the target of quenching by LHCSR.

INTRODUCTION

Light is essential for photosynthesis and yet too much is potentially harmful. Excess photons increase the amount of singlet chlorophyll (^{1}Chl*) and, thus, the probability for formation of triplet chlorophyll (^{3}Chl*) and singlet oxygen ($^1O_2$), with consequent photoinhibition that limits growth. Oxygenic organisms have evolved different photoprotective mechanisms in order to avoid the formation of reactive oxygen species, including triplet quenching (Dall'Osto et al., 2012; Ballottari et al., 2013), reactive oxygen species scavenging (Baroli et al., 2003; Dall'Osto et al., 2010), and alternative electron transport pathways (Cardol et al., 2011). In addition to these constitutive mechanisms, a rapidly inducible process known as nonphotochemical quenching (NPQ) is activated within seconds upon exposure to excess light and then catalyzes thermal dissipation within the photosystem II (PSII) antenna system (Niyogi and Truong, 2013; de Bianchi et al., 2010).

In plants, Photosystem II Subunit S (PSBS), a member of the light-harvesting complex superfamily (LHC) depleted in chlorophyll binding motifs (Dominici et al., 2002), is a sensor for low lumenal pH (Li et al., 2000). Its protonation causes a conformational change that is propagated to LHC proteins of PSII, leading to dissociation of outer antenna complexes from PSII supercomplexes and clustering of peripheral LHCII (Bonente et al., 2008a; Betterle et al., 2009; Johnson et al., 2011). This causes quenching at two sites: Q1 (zeaxanthin-independent) located in LHCII clusters and Q2 (zeaxanthin-dependent) within supercomplexes (Ballottari et al., 2013).

In green algae, Light-Harvesting Complex Stress-Related (LHCSR) (Peers et al., 2009; Niyogi and Truong, 2013), rather than PSBS (Bonente et al., 2008b; Niyogi and Truong, 2013), is essential for NPQ. LHCSR senses pH via lumen-exposed protonatable residues, as does PSBS. However, LHCSR binds both chlorophyll and xanthophylls and exhibits a short fluorescence lifetime that is even shorter at low pH (Bonente et al., 2011; Liguori et al., 2013). Consistent with this, a PSII-LHCII-LHCSR3 supercomplex from high-light-grown *Chlamydomonas reinhardtii* cells was recently reported (Tokutsu and Minagawa, 2013). Although LHCSR and PSBS have received much attention for their essential role in triggering NPQ, their localization in thylakoid domains is not known. PSBS has been purified from grana preparations in which PSII and its antenna are localized (Funk et al., 1994; Harrer et al., 1998), consistent with its control over PSII fluorescence. LHCSR localization is still unclear due to the difficulty of isolating grana domains from unicellular algae (Bergner et al., 2015).

In *Physcomitrella patens*, a moss species early divergent from the green algae to plant lineage, both PSBS and LHCSR proteins are active (Rensing et al., 2008; Alboresi et al., 2010). *P. patens* represents a basal lineage of land plants that diverged before the acquisition of well developed vasculature. Thus, it stands in an important phylogenetic position for illuminating the evolutionary development of vascular plants, including model organisms such

[1] Current address: Department of Biology, University of Padova, Via Ugo Bassi 58/B, 35121 Padova, Italy.
[2] Address correspondence to roberto.bassi@univr.it.
The author responsible for distribution of materials integral to the findings presented in this article in accordance with the policy described in the Instructions for Authors (www.plantcell.org) is: Roberto Bassi (roberto.bassi@univr.it).
www.plantcell.org/cgi/doi/10.1105/tpc.15.00443

as *Arabidopsis thaliana*. Here, we show that LHCSR is localized in stroma-exposed membranes and PSBS is associated with grana partitions. LHCSR regulates both photosystem I (PSI) and PSII fluorescence, but PSBS is active on only PSII. These results are interpreted in light of the high LHCII abundance in the stroma membranes, in which it acts as a functional antenna for PSI. We propose that LHCSR independently catalyzes quenching of PSII-LHCII in grana membranes and on PSI-LHCI-LHCII complexes in stroma exposed domains. Such a mechanism not only allows control of excitation in both PSI and PSII antenna systems but also promotes maintenance of the plastoquinone (PQ) redox poise in the absence of PSI far-red absorption forms, which are low in mosses and unicellular algae and are fully developed in higher plants.

RESULTS

NPQ Activity in *Physcomitrella patens* from Both LHCSR and PSBS Can Be Detected by Fluorescence Measurement at Room Temperature and 77K

The *P. patens* genome contains two *lhcsr* genes and one *psbs* gene whose products are all independently active (Alboresi et al., 2008, 2010; Rensing et al., 2008) as shown in Figure 1. Figure 1A shows a transmittance image (top) of an agar plate culture with four moss genotypes. Fluorescence images of the same plate that was dark-adapted (lower left) and then treated to high light (HL; lower right) show that wild-type plants undergo stronger light-induced fluorescence quenching compared with knockout (KO) mutant plants lacking either LHCSR1 and 2 (*lhcsr* KO), PSBS (*psbs* KO), or all three proteins (*npq4*). Immunoblot analysis (Figure 1B) shows that an α-LHCSR1 antibody detected two closely migrating bands at 23 and 23.5 kD, the lower band corresponding to LHCSR2, whereas an α-PSBS antibody revealed a single 22-kD band. None of the three bands was detected in the triple mutant *lhcsr1* × *lhcsr2* × *psbs* KO (hereafter referred to as *npq4*). Both LHCSR1 and 2 bands were missing in the *lhcsr1* × *lhcsr2* KO strain (*lhcsr* KO) but were retained in *psbs* KO, which, in turn, lacked the 22-kD band. Figure 1C shows pulse fluorometry time courses upon illumination of *P. patens* wild-type and mutant strains with saturating light. Following an 8-min illumination, F_{max} was decreased by ~80% (NPQ = 3.8) in the wild type, whereas both *psbs* KO and *lhcsr* KO showed reduced fluorescence quenching (NPQ = 2.5 and 0.7, respectively). No quenching was detected in *npq4*. Room temperature (RT) fluorescence mainly derives from PSII (Cho et al., 1966). Figure 1D shows that the quenched conformation induced by HL was preserved by rapidly freezing the moss protonematal tissue in liquid nitrogen. Upon excitation of the chlorophyll *b*-rich antenna system at 475 nm, the 77K fluorescence emission spectra of either dark-adapted or HL-treated samples yielded three peaks: 717, 682, and 693 nm (arising from PSI-LHCI, LHCII, and PSII core, respectively). Upon normalization to PSI emission, the

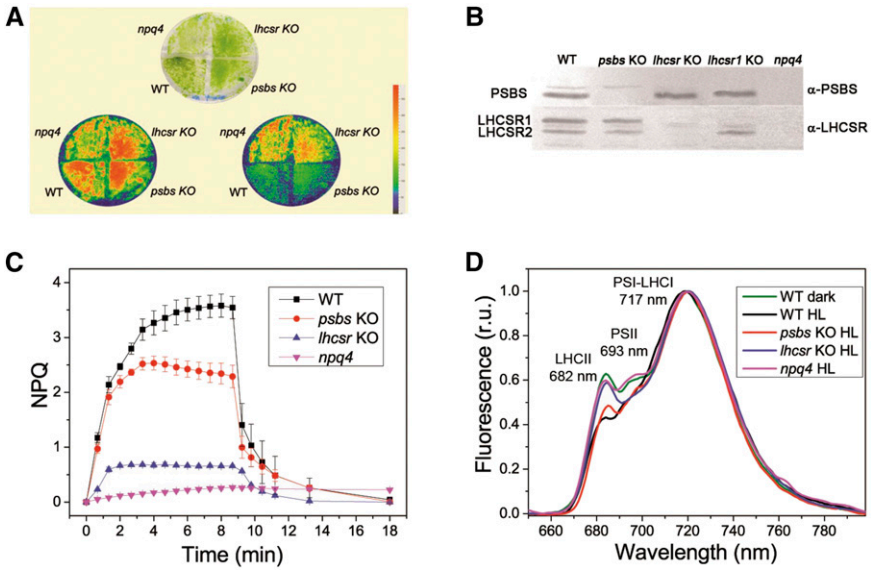

Figure 1. Fluorescence Imaging Analysis of NPQ Activity of Wild-Type *P. patens* and Mutants Lacking PSBS (*psbs* KO), LHCSR1 and 2 (*lhcsr* KO), or All the Three Proteins (*npq4*).

(A) Transmittance image (top) of *P. patens* wild type plus *psbs* KO, *lhcsr* KO, and *npq4* mutants grown in Petri plates on solid medium. Fluorescence images (bottom) of the four strains at F_{max} (left) and F'_{max} (right) upon 10 min HL treatment (850 μmol photons m^{-2} s^{-1}) at RT.

(B) Immunoblotting analysis using antibodies directed against PSBS or LHCSR. One microgram of chlorophyll of thylakoids was loaded in each lane.

(C) Pulse-amplitude fluorimetric time course at RT: Dark-adapted plants that were exposed to HL (850 μmol photons m^{-2} s^{-1}) for 8 min and then left to recover for further 10 min in the dark. Data are expressed as mean ± SD (n = 3).

(D) Fluorescence spectra at 77K of *P. patens* protonemal tissues, either dark adapted (dark) or following illumination for 10 min with HL (850 μmol photons m^{-2} s^{-1}). Spectra were normalized to PSI emission at 717 nm. Excitation was at 475 nm. Dark-adapted spectra of mutant tissues did not show significant differences with respect to the wild type and are not shown.

Table 1. Chlorophyll *a*/*b* Ratio of Thylakoids and dG, dM, dS, and yS Fractions Obtained from Digitonin and Yeda Press Preparations of Arabidopsis and *P. patens* and of the PSI-LHCI Complex Obtained by Sucrose Gradient Ultracentrifugation (Supplemental Figure 1A)

Species	Thylakoids	dG	dM	dS	yS	PSI-LHCI
P. patens	2.45 ± 0.14	2.09 ± 0.04	2.24 ± 0.03	3.23 ± 0.08	3.63 ± 0.23	6.86 ± 0.58
Arabidopsis	2.90 ± 0.10	2.22 ± 0.02	2.10 ± 0.02	4.12 ± 0.11	5.88 ± 0.11	6.60 ± 0.15

Data are expressed as mean ± SD (n = 3).

decrease in the amplitude of the latter components in HL is consistent with quenching in PSII antenna system.

Fractionation of Thylakoid Membrane Domains of *P. patens* versus Arabidopsis by Digitonin and Yeda Press

The observation that quenching by PSBS and LHCSR are additive suggests that they might act on at least partially distinct pigment beds. In order to test this hypothesis, we studied the organization and lateral heterogeneity of thylakoid membranes in *P. patens* by assessing the distribution of antigens among different membrane domains, including, as a reference, the well characterized higher plant Arabidopsis. We fractionated the thylakoid membranes by three complementary methods. The most comprehensive and widely used procedure involves solubilization with digitonin and differential centrifugation (Barbato et al., 2000; Sirpiö et al., 2007), yielding three fractions: grana, stroma, and grana margins (dG, dS, and dM, respectively). In addition, a method specific for isolation of stroma membranes was also reported by mechanical fractionation using Yeda press (yS) (Bassi et al., 1988a) as well as one yielding grana partition membranes (Morosinotto et al., 2010). Chlorophyll *a*/*b* ratios of the dG, dM, and dS fractions were 2.09 ± 0.04, 2.24 ± 0.03, and 3.23 ± 0.08, respectively. The yS fraction was further enriched in chlorophyll *a* (chlorophyll *a*/*b* = 3.63 ± 0.23) with respect to *P. patens* thylakoids (chlorophyll *a*/*b* = 2.45 ± 0.14) as shown in Table 1. SDS-PAGE analysis of these fractions showed that the dG fraction was enriched in the PSII core proteins CP43 and CP47 but was depleted in PSI polypeptides such as PSAA/B, LHCI, and ATPase subunits (Figure 2A). The dM fraction contained both PSI and PSII markers but little ATPase, which, in turn, was enriched in dS and yS fractions together with PSI. The properties of the fractions from Arabidopsis were very similar but for the remarkable difference that the chlorophyll *a*/*b* ratio of the stroma membrane-derived fractions (dS and yS) was 4.12 and 5.88, respectively, thus clearly higher than the corresponding fractions from *P. patens*, which scored 3.23 and 3.63 (Table 1). Immunoblot analysis using α-PSI- and α-PSII-specific antibodies confirmed the lateral heterogeneity of PSI versus PSII in *P. patens* membrane domains as well as Arabidopsis, consistent with previous work (Tikkanen et al., 2012) (Figure 2B). In addition, the reaction of an antibody against CP29, which is closely associated with the PSII core complex (Harrer et al., 1998), was stronger in dG, less in dM, much less in dS, and below detection in the yS fraction, consistent with PSII and its interactors partitioning in grana domains. Thus, lateral segregation of PSI versus PSII was similar in the moss and the higher plant (Figure 2A) and yet the stroma-membrane-derived fractions were enriched in chlorophyll *b*. Figures 2A and 2C (arrows) show that this was due to a higher LHCII content that was not accompanied by PSII core complexes (Figures 2B and 2C), suggesting that LHCII might be localized in stroma lamellae in *P. patens* to a greater extent than in plants.

Functional Antenna Size of PSI

We verified whether this LHCII population was part of the PSI antenna by measuring the kinetics of P700 oxidation. As shown in Figure 2G, we observed more rapid $P700^+$ formation in *P. patens* ($T_{2/3}$ = 0.45 ± 0.04*10^3 ms^{-1}) versus Arabidopsis ($T_{2/3}$ = 0.27 ± 0.04*10^3 ms^{-1}). As a reference, we measured the oxidation kinetics of isolated PSI-LHCI complexes purified from either *P. patens* or Arabidopsis thylakoids upon *n*-dodecyl-α-D-maltoside (α-DM) solubilization and sucrose gradient ultracentrifugation (Supplemental Figure 1). This exhibited the same $T_{2/3}$ of P700 photooxidation ($T_{2/3}$ = 0.28 ± 0.07*10^3 ms^{-1}) regardless of the species (Figure 2H). Because the chlorophyll *a*/*b* ratio of purified PSI-LHCI complexes was ~6.7 in both *P. patens* and Arabidopsis, the difference in chlorophyll *b* content and antenna size was due to enrichment in LHCII, as detected by SDS-PAGE and green gel analysis (Figures 2A and 2C). Further verification was obtained by immunoelectron microscopy analysis of moss versus plant tissues using an α-LHCII-specific antibody (Figures 2E and 2F). Primary antibodies were imaged using a colloidal gold-coupled secondary antibody. The ratio of α-LHCII-bound gold particles detected in exposed versus stacked membranes was 1.2 in *P. patens* versus 0.5 in Arabidopsis (Figure 2D). Thus, in the moss, ~50% of the LHCII label was located in stroma-exposed membranes together with PSI.

Distribution of PSBS and LHCSR upon Fractionation by α-DM

Immunoblot analysis of PSBS and LHCSR in these thylakoid fractions indicated that their distribution was complementary to each other: PSBS was enriched in grana-derived fractions and hardly detectable in stroma membranes, whereas LHCSR was enriched in stroma membranes and was minimally present, if at all, in grana-derived fractions (Figure 2B). For a more precise determination of the relative abundance of LHCSR and PSBS with respect to PSI and PSII, we titrated these four antigens in membrane fractions (Supplemental Figure 2). The results, summarized in Figures 3A to 3D, show that the grana-derived fraction (dG) had high levels of PSII and PSBS but low levels of LHCSR, whereas stroma-membrane-derived fractions had high levels of PSI and LHCSR but low levels of PSBS. The dM (grana margins) included both PSBS and LHCSR, although they were less enriched than in grana and stroma membranes, respectively. Further support for a granal/stromal membrane localization of PSBS/LHCSR was provided by step solubilization of stacked thylakoids

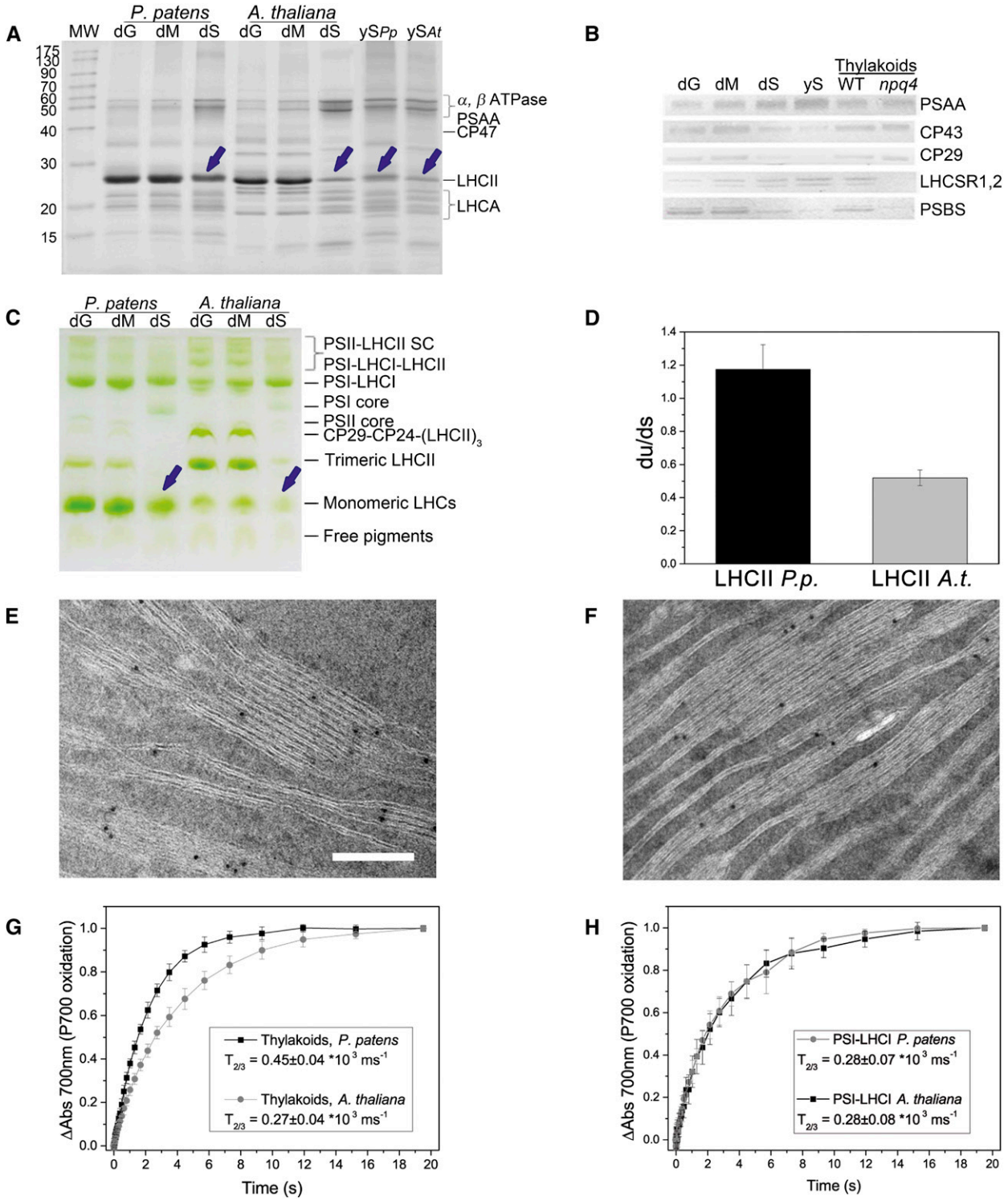

Figure 2. Organization of Arabidopsis and *P. patens* Thylakoid Membranes.

(A) SDS-PAGE analysis of Arabidopsis and *P. patens* thylakoids and fractions obtained by digitonin or Yeda press fractionation. Bands corresponding to PSI, PSII, and ATPase are indicated on the right side of the gel. A molecular weight marker (MW) is shown on the left. Arrows highlight the 25-kD band of LHCII in the stroma fractions from *P. patens* and Arabidopsis. Each lane was loaded with 3 μg chlorophyll. yS, stroma-exposed membranes obtained by Yeda press fractionation; dG, dM, and dS, grana, grana margins, and stroma-exposed membranes obtained using digitonin.

with α-DM showing preferential extraction of PSI and LHCSR versus PSBS and PSII, which remained in the pellet fraction constituted by grana partitions (Supplemental Figures 3 and 4).

Immunolocalization of LHCSR and PSBS in Intact Chloroplasts

Biochemical analysis clearly supported a stromal-exposed thylakoid domain localization for LHCSR. Yet, its quenching activity of PSII fluorescence (Figures 1A, 1C, and 1D) appeared to contradict this finding because PSII was clearly localized in grana partitions in *P. patens* (Figures 2 and 3), as previously reported for higher plants (Andersson and Anderson, 1980). We thus proceeded to a direct assessment of these antigens by immunoelectron microscopy localization in intact *P. patens* tissues using antibodies against PSBS and LHCSR as well as PSBO (the 33-kD oxygen-evolving complex subunit [OEC]) and CP43, the last two being components of the PSII core complex. Although we assayed several α-PSI antibodies with *P. patens*, none has showed an avid and specific labeling of electron microscopy sections. Indeed, only one out of the six antibodies we tested was appropriate for immunoblotting and may be explained by reports of multiple isoforms for PSI subunits in moss (Busch et al., 2013). The distribution was normalized for the relative abundance of stacked versus unstacked membranes in the chloroplasts (du/ds score), which was 65% ± 0.5% through all sets of micrographs. The distribution of CP43 and OEC antigens was strongly biased against stroma-exposed membranes with du/ds scores in the range of 0.1 to 0.3. LHCSR and PSBS had a du/ds value of 4.1 and 1.0, respectively (Figure 3I). This confirmed that PSBS is essentially localized in grana stacks even if its segregation is somewhat less extreme with respect to that of the PSII core complex. LHCSR, instead, was highly enriched in stroma-exposed membranes. In summary, the above findings show that although LHCSR is a fluorescence modulator of PSII located in the grana, it primarily resides in the stroma membranes and, to a lesser extent, in the grana margins.

LHCSR Does Not Change Localization upon High-Light Treatment

Possible explanations for the effect of LHCSR on PSII fluorescence (Figure 1) include either that there is a reversible change in its thylakoid domain distribution upon induction of NPQ, a process previously described for LHCII during state transitions (Bassi et al., 1988b; Depège et al., 2003; Nevo et al., 2012), or that LHCSR exerts its function within the stroma membranes. To examine the first possibility, we exposed intact chloroplasts (20 μg/mL chlorophyll) either to control light (50 μmol photons m^{-2} s^{-1}) that was unable to induce NPQ or to saturating light (850 μmol photons m^{-2} s^{-1}) for 10 min. This elicited a strong, reversible, NPQ activity (Figure 4A), after which detergent (α-DM) was added to different concentrations to isolate thylakoids in a grana-enriched pellet from a stroma membrane-enriched supernatant (Morosinotto et al., 2010). These fractions showed no significant NPQ-dependent changes between pellet and supernatant regarding chlorophyll distribution, chlorophyll *a*/*b* ratio (Table 2), or PSAA and CP43 content (Figures 4C and 4D). This strongly suggests that *P. patens* thylakoids did not undergo significant changes in their level of stacking, antenna versus reaction center ratio or PSI/PSII ratio. Also, the localization of LHCSR was the same, regardless of whether NPQ was triggered or not (Figure 4B; Supplemental Figure 5), implying that LHCSR did not shuttle between grana and stroma lamellae. In the mild conditions used in this experiment, a clear pattern emerged with three steps of LHCSR content in the pellet fraction, namely, 80% or more below 0.08% α-DM, 40% with 0.13% > α-DM < 0.32%, and <10% above 0.32% α-DM.

We then analyzed the pellet fraction by transmission electron microscopy following negative staining (Figures 4E to 4H). Samples obtained at the lowest detergent concentrations consisted of aggregated, partially solubilized thylakoids with both grana and stroma membrane domains, as identified from the size and density of stain-excluding particles (0.08% α-DM or below). Between 0.13 and 0.32% (intermediate α-DM concentrations), grana vesicles including sealed margins were observed. At 0.32% or above, mainly coupled grana disks with exposed membrane sections were observed. Only a very small fraction of membrane disks exhibited paired membrane layers exposed at α-DM <0.16%, whereas this was by far the most represented form at α-DM 0.32%. A significant number of grana disks were partially disrupted at 0.39% α-DM. Based on these observations, we suggest that LHCSR partitioned into two of three thylakoid membrane domains, namely, stroma membranes and grana margins, whereas grana partitions were essentially depleted of LHCSR. From the amplitude of the residual LHCSR signal in the pellet fractions at low detergent (Figure 4B), the relative size of the

Figure 2. (continued).

(B) Immunoblot analysis of *P. patens* thylakoid membrane fractions from digitonin or Yeda press treatment (0.5 μg chlorophyll per lane). Thylakoids of the wild type and *npq4* are also shown as controls. The immunoblots were probed with α-PSAA, α-CP43, α-CP29, α-LHCSR, and α-PSBS antibodies.
(C) Deriphat-PAGE analysis of selected thylakoid membrane fractions obtained by digitonin treatment. Samples were solubilized with 1% *n*-dodecyl-β-maltoside (β-DM). Bands corresponding to different green complexes are indicated on the right side of the gel. Arrows indicate the LHCII band of monomeric LHC antenna proteins in the stroma membrane fraction of *P. patens* and Arabidopsis stroma membranes.
(D) Distribution of gold particles coupled to LHCII-specific antibody between grana and stroma-exposed membranes calculated as described in Methods. The du/ds ratio compares relative labeling in unstacked versus stacked membranes in the chloroplasts. Data are reported as mean ± SD. Numbers of images/particles analyzed were as follows: Arabidopsis, 51/1199; and *P. patens*, 61/1299.
(E) and **(F)** Representative transmission electron microscopy images of thylakoid membranes labeled with antibodies against LHCII in Arabidopsis **(E)** or *P. patens* **(F)**. Both images are at the same magnification. Bar = 200 nm.
(G) and **(H)** Kinetics of $P700^+$ formation in *P. patens* and Arabidopsis thylakoids **(G)** and isolated PSI-LHCI complexes **(H)**. Data are reported as mean ± SD. Measurement conditions are described in Methods.

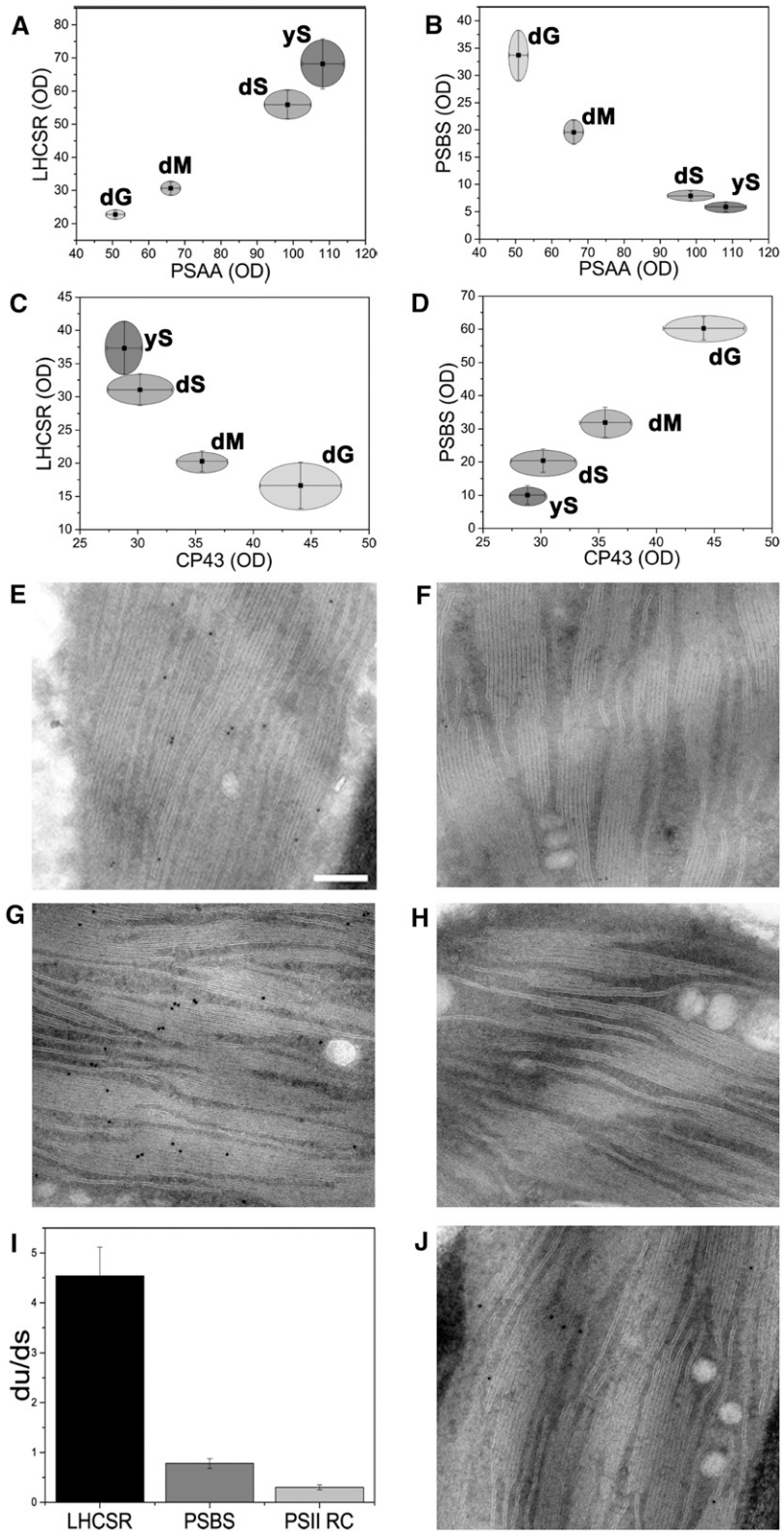

Figure 3. Distribution of LHCSR and PSBS between *P. patens* Thylakoid Membrane Domains.

two pools can be estimated as 70% in stroma-exposed membrane domains and 30% in grana margins.

NPQ Dissection of PSII versus PSI by 77K Fluorescence Spectroscopy

The localization of LHCSR in the stroma membranes together with PSI-LHCI complexes suggests that there might be an effect on PSI excited states besides that observed with PSII (Figures 1A, 1C, and 1D). Because PSI fluorescence yield is very low at RT, we devised a method for the analysis of both PSI and PSII at low temperature (LT), a condition in which both PSI and PSII have high fluorescence yield (Cho et al., 1966). We used intact chloroplasts active in NPQ (Figure 4A). Chloroplasts, either dark-adapted or illuminated for 10 min, were rapidly frozen in liquid nitrogen (the HL sample done directly under the light) and fluorescence emission spectra were recorded. GFP (1 μM) was added to the chloroplast suspension just before the treatment as an internal standard. Figures 5A to 5D show the fluorescence emission spectra of dark-adapted versus HL-treated chloroplasts in the 495- to 800-nm range, including the 513-nm peak of GFP to which the signal was normalized. In the wild type, upon the HL treatment, the amplitude of the spectrum was decreased throughout the whole range, with preference for PSII components (682 and 693 nm) (Figure 5A). The extent of quenching was reduced in *psbs* KO (Figure 5C) and further reduced in the *lhcsr* KO and *npq4* (Figures 5B and 5D) mutants. These differences, consistent with the effect observed in vivo (Figures 1C and 1D) indicated this technique is efficient in detecting NPQ-derived fluorescence changes. In addition, it was possible to detect quenching specifically for the PSI component (717 nm) in the wild type and *psbs* KO, which both harbor LHCSR.

By contrast, genotypes lacking LHCSR, namely, *lhcsr* KO and *npq4*, did not exhibit the PSI-specific quenching. The LT spectra of *lhcsr* KO and *npq4* were similar and yet there were indications that the quenching observed in these two genotypes had different origins, as suggested by the kinetics of fluorescence recovery in the PAM fluorometry measurements. Although *lhcsr* KO exhibited prompt recovery in the dark, *npq4* did not, implying photoinhibition (Figure 4A). In order to discriminate between genuine qE and slower inhibitory components, namely, qZ or qI (Dall'Osto et al., 2005; Kalituho et al., 2007; Ballottari et al., 2013), we isolated the rapid qE component of NPQ by freezing samples at different times up to 6 min under HL and following further incubation in dark for up to 5 min to allow for selective relaxation of only qE (Figures 5E and 5F; Supplemental Figure 6). Dark-recovered (5 min) minus light-only (6 min) difference spectra, depicted in Figure 6A, show that whereas *lhcsr* KO chloroplasts underwent quenching of only the PSII component, both *psbs* KO and wild-type chloroplasts quenched both PSI and PSII emissions. The *npq4* mutant, lacking both LHCSR and PSBS, showed a negative difference spectrum consistent with the effects of photoinhibition, as no fluorescence recovery was observed upon returning the chloroplasts of this genotype in the dark (Figure 4A). We conclude that PSBS acts only on PSII excited states, while LHCSR acts on both PSI and PSII. The above finding raises the question of whether the quenching of PSI occurs with the same kinetics as those of PSII. To assess this, we froze wild-type chloroplasts in a time-course experiment during illumination and analyzed the 77K fluorescence emission spectra for the amplitude of the PSII and PSI components, deconvoluted as described in Methods. After plotting these amplitudes (Figure 6B), we observed that PSII was quenched first, followed by PSI, which, in turn, recovered its fluorescence faster and more completely in the dark.

Finally, we asked which component of the photosynthetic apparatus was primarily quenched by LHCSR. To this aim, we illuminated isolated chloroplasts to induce quenching and, thus, the interaction between LHCSR and its target protein. Chloroplasts were then solubilized with 0.8% α-DM at either pH 7.0 or 5.0, and the pigment-proteins were fractionated by sucrose gradient ultracentrifugation at either of the pH conditions. LHCSR was found in the upper gradient fraction together with monomeric LHC proteins independent of the treatment and pH of the separation, implying that the interactions of LHCSR with other thylakoid components were weak and did not survive solubilization with α-DM. In another experiment, we recorded LT fluorescence excitation spectra for PSI emission (717 nm) of the wild type in the quenched state or upon recovery in the dark. The spectra are shown in Figures 6C and 6D, along with the spectrum of the *P. patens* PSI-LHCI complex isolated from sucrose gradient ultracentrifugation (Supplemental Figure 1). The chlorophyll *b* contribution to PSI emission in the unquenched chloroplasts was enhanced compared with that of isolated PSI-LHCI complex, but this difference decreased following the HL treatment (Figure 6C). In the *lhcsr* KO mutant, however, no decrease in chlorophyll *b* contribution was observed (Figure 6D), implying that the contribution of a chlorophyll *b*-rich complex, most likely LHCII, to the

Figure 3. (continued).

(A) to **(D)** Quantification of LHCSR and PSBS versus PSI or PSII RC subunits from digitonin/Yeda press thylakoid fractions. Scatterplots compare the distribution of PSBS and LHCSR versus CP43 or PSAA. Different amounts of yS, dG, dM, and dS were fractionated by SDS-PAGE, transferred to polyvinylidene fluoride membranes, and probed with specific antibodies. The optical density (OD) signal from the immune reaction was normalized to the same chlorophyll amount. Data are reported as mean ± SD ($n = 4$ to 6). Representative images of the immunoblot analysis are shown in Supplemental Figure 2. yS, stroma-exposed membranes obtained by Yeda press fractionation; dG, dM, and dS, grana, grana margins, and stroma-exposed membranes obtained by digitonin.

(E) to **(H)** Distribution of LHCSR and PSBS within the thylakoid membranes of *P. patens*. Shown are representative images of thylakoid membranes labeled with antibodies against LHCSR (**[E]** and **[F]**) or PSBS (**[G]** and **[H]**), in wild-type (**[E]** and **[G]**), *lhcsr*-deficient **(F)**, or *psbs*-deficient **(H)** strains. All transmission electron micrographs are at the same magnification. Bar = 200 nm.

(I) Distribution of gold particles coupled to LHCSR-, PSBS-, PSBO-, and CP43-specific antibodies between grana- and stroma-exposed membranes calculated as described in Methods. The du/ds ratio compares relative labeling in unstacked versus stacked membranes in the chloroplasts. Data are reported as means ± SD. Number of images/particles analyzed was as follows: LHCSR, 86/1183; PSBS, 58/1287; and PSBO+CP43, 113/620.

(J) Distribution of PSII RC within the thylakoid membranes of *P. patens*. Image shows thylakoid membranes labeled with antibodies against PSBO.

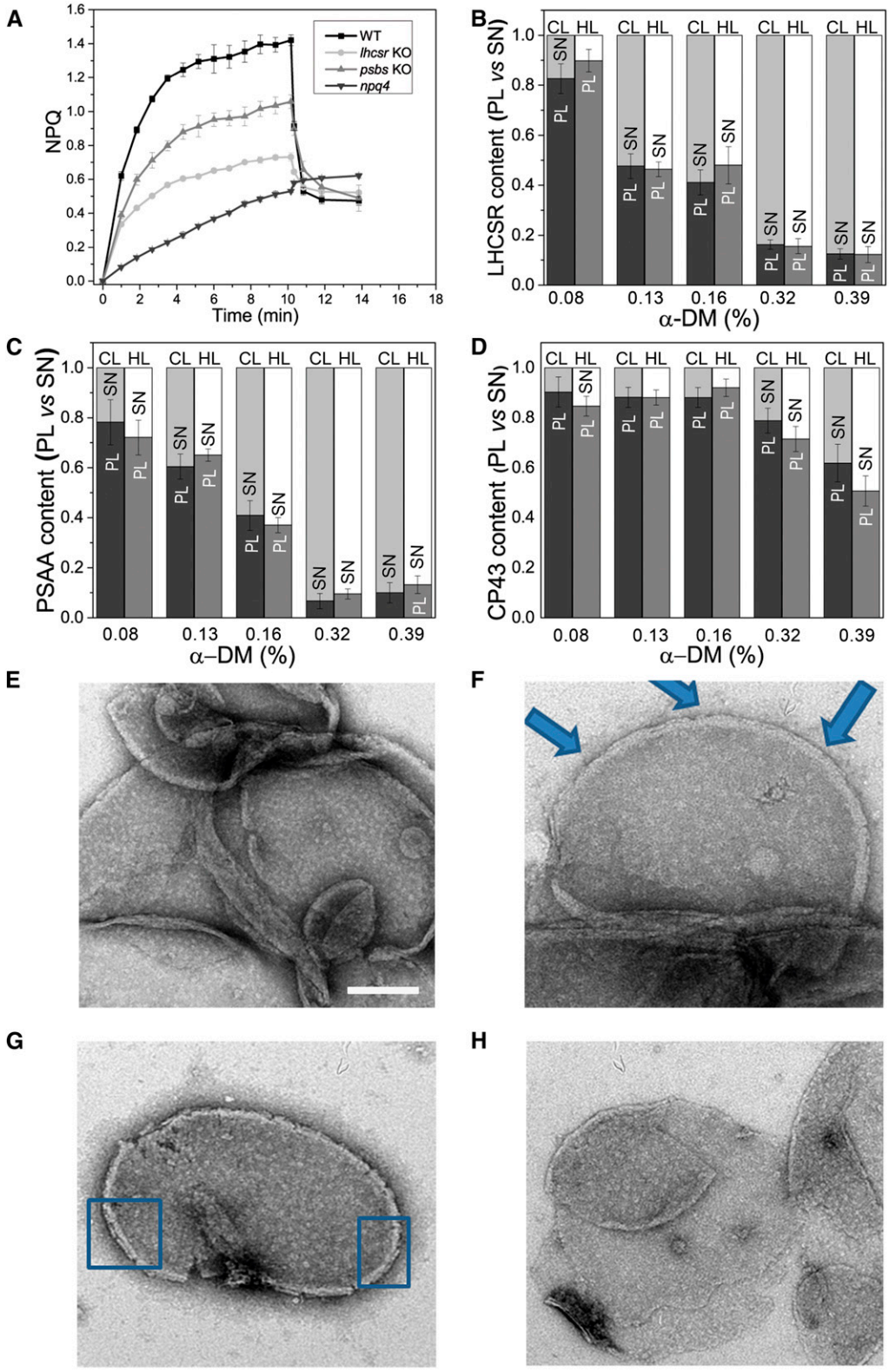

Figure 4. Invariance of LHCSR Distribution in Pellet versus Supernatant Fractions upon Illumination with Either Control Light, Yielding No NPQ, or HL, Causing NPQ.

Table 2. Chlorophyll Content (μg) and Chlorophyll *a/b* Ratio in Supernatant and Pellet after Fractionation of Intact Chloroplasts upon Exposure for 10 min to Either Control Light or HL

		0.08		0.13		0.16		0.32		0.39	
	α-DM (%)	CL	HL	CL	HL	CL	HL	CL	HL	CL	HL
SN	μg Chl	38.75	37.21	62.51	75.2	85.41	87.5	147.61	170.84	159.92	195.21
	Chl *a/b*	2.70 ± 0.11	2.89 ± 0.15	2.37 ± 0.10	2.2 ± 0.20	2.63 ± 0.20	2.40 ± 0.11	2.53 ± 0.09	2.25 ± 0.10	2.37 ± 0.12	1.71 ± 0.15
PL	μg Chl	161.25	163.41	146.02	123.91	126.32	125.05	76.11	62.43	61.52	39.23
	Chl *a/b*	2.19 ± 0.15	2.05 ± 0.12	2.13 ± 0.15	2.01 ± 0.17	2.02 ± 0.10	1.94 ± 0.12	1.83 ± 0.13	1.62 ± 0.11	1.56 ± 0.10	2.09 ± 0.20

After either treatment, α-DM was added to a final concentration of 0.08 to 0.39%, and pellet versus supernatant fractions were harvested by centrifugation at 40,000*g*. SN, supernatant; PL, pellet; CL, control light (50 μmol photons m^{-2} s^{-1}); HL, high light (850 μmol photons m^{-2} s^{-1}); Chl, chlorophyll.

PSI excited state concentration was modulated by the activity of the LHCSR proteins.

DISCUSSION

Although excess energy dissipation has been studied for over 40 years, the mechanistic details of this process are far from clear. Besides the mechanism catalyzed by PSBS in plants, a distinct mechanism operates in unicellular algae via LHCSR (Bonente et al., 2008a; Peers et al., 2009). Critical information for the elucidation of the mechanism of NPQ involves the sites of quenching within the thylakoid membrane domains and the identity of photosystem subunits interacting with the pH sensing proteins PSBS and LHCSR. Also, we would like to understand the reasons why LHCSR was replaced by PSBS during evolution upon the transition from aquatic to terrestrial life forms. The discovery that both PSBS and LHCSR are active in *P. patens* offers the possibility of a comparative study of LHCSR and PSBS-dependent mechanisms in the same physiological and structural context.

Here, we have determined that, in moss, as in higher plants (Andersson and Anderson, 1980; Simpson, 1983), PSI and PSII are strictly confined to the stroma lamellae and grana stacks, respectively, whereas LHCII is abundant in both membrane domains (Figures 2A and 2C to 2F) and is functionally connected to the PSI-LHCI complex, thus doubling its antenna size compared with isolated PSI-LHCI (Figures 2G and 2H). Based on the figure of 178 chlorophyll/PSI-LHCI (Bassi et al., 1988a; Ben-Shem et al., 2003; Mazor et al., 2015) versus 42 chlorophyll/LHCII trimer (Dainese and Bassi, 1991; Liu et al., 2004), the PSI functional antenna size of mosses includes four LHCII trimers versus five LHCII trimers per PSII. In this context, the observation that PSBS colocalizes with PSII in grana partitions whereas LHCSR is found in both stroma membranes and grana margins, both in quenched and unquenched conditions (Figures 3 and 5), implies that PSBS and LHCSR proteins act on PSII and PSI + PSII, respectively. We show that the quenched conformation can be preserved by rapidly freezing the HL-treated tissues at liquid nitrogen (Figures 1D and 5), allowing for independent assessment of changes in PSI and PSII fluorescence yield when using GFP as an internal standard. This technical improvement allowed us to determine contributions to the fluorescence emission spectra of PSI distinct from those of PSII, a feat difficult to achieve at RT due to the low yield of PSI emission at this temperature (Cho et al., 1966). In our hands, GFP proved to be a far better internal standard than fluorescein, which was previously proposed (Krause et al., 1983), yielding highly reproducible results. This allowed us to establish that LHCSR modulates both PSI and PSII fluorescence.

Previous work has shown that LHCSR3 interacts with the PSII-LHCII supercomplex in *C. reinhardtii* (Tokutsu and Minagawa, 2013) and that this interaction is stabilized by PSBR (Xue et al., 2015) but might undergo interaction with PSI-LHCI-FNR in the absence of STT7-dependent phosphorylation (Bergner et al., 2015). However, it should be noted that lack of STT7 did not prevent NPQ at RT (Bonente et al., 2011). In *P. patens*, we did not detect LHCSR phosphorylation upon exposure to HL or transition between PSI and PSII lights (data not shown), whereas thylakoid fractionation in HL versus CL did not show changes in the distribution of this protein between thylakoid domains (Figure 4B; Supplemental Figure 5), indicating that LHCSR exerts its function in the two thylakoid domains in which it resides, namely, the

Figure 4. (continued).

(A) Kinetics of NPQ as measured by PAM fluorometry on isolated chloroplasts of different genotypes. Illumination was with 850 μmol photons m^{-2} s^{-1} (HL) for 10 min, followed by 4 min of recovery in the dark. Data are reported as mean ± SD ($n \geq 3$).

(B) to **(D)** Distribution of LHCSR **(B)**, PSAA **(C)**, and CP43 **(D)** between pellet and supernatant fractions that were obtained by treating the chloroplast suspension (20 μg chlorophyll/mL) with different α-DM concentrations followed by centrifugation al 40,000*g*. Black, control light pellet; light gray, control light supernatant; dark gray, HL pellet; white, HL supernatant. Data are expressed as mean ± SD ($n = 3$). CL, control light (50 μmol photons m^{-2} s^{-1}); HL, high light; PL, pellet; SN, supernatant.

(E) to **(H)** Electron microscopy negative staining images of pellet (grana-derived particles) obtained with different α-DM concentrations: **(E)** 0.08% α-DM, **(F)** 0.13% α-DM, **(G)** 0.32% α-DM, and **(H)** 0.39% α-DM. Arrows in **(F)** indicate the rounded grana edges attributed to margins. Squares in **(G)** highlight the paired membrane edges corresponding to grana partitions upon trimming of the "margins." No significant differences were observed between control light and HL samples. All transmission electron micrographs are at the same magnification. Bar = 100 nm.

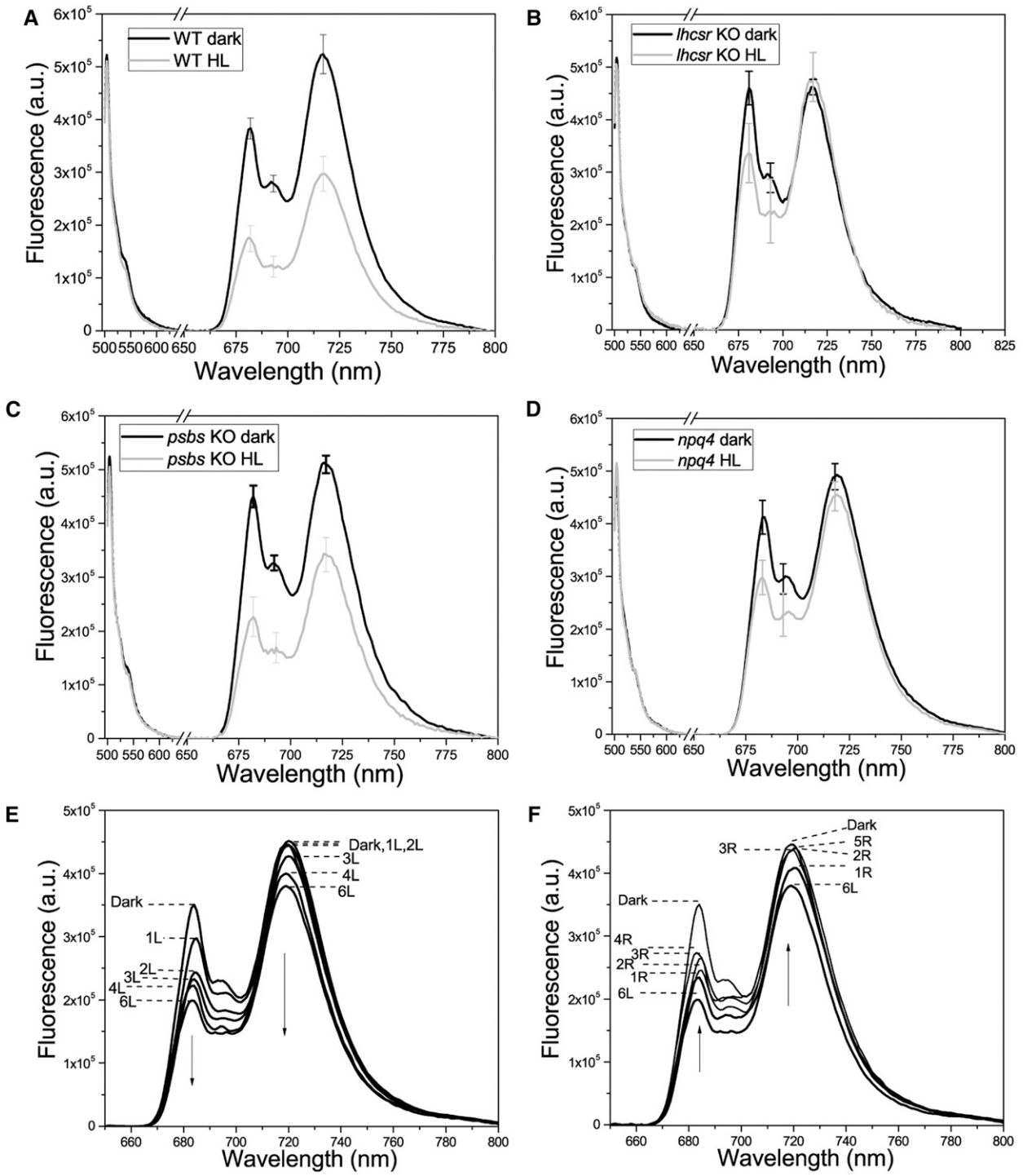

Figure 5. Measurement of Quenching Induced by HL in Isolated Chloroplasts from *P. patens* Wild-Type and Mutant Strains by 77K Fluorescence Emission Spectroscopy.

(A) to **(D)** The 77K fluorescence emission spectra of *P. patens* wild-type **(A)**, *lhcsr* KO **(B)**, *psbs* KO **(C)**, and *npq4* **(D)** intact chloroplasts that were either maintained in the dark (black) or exposed to 850 µmol photons m^{-2} s^{-1} for 10 min (gray) before rapidly freezing in liquid nitrogen. GFP (1 µM) was added to the chloroplast suspension as an internal standard. Spectra are reported as mean of three independent measurements; each measure is the average of at least 10 records. To simplify the view, mean ± SD was indicated only at the peaks for PSII (682 and 693 nm) and PSI (717 nm).

(E) and **(F)** The 77K spectra as in **(A)** to **(D)** but exposed to HL for different times (L) or exposed for 6 min and then recovered for different times in the dark (R). Arrows indicate the direction on changes in the amplitude of the peaks. Spectra were obtained upon excitation at 475 nm were normalized to the amplitude of the 513-nm emission peak of GFP.

stroma-exposed membranes and grana margins (Figures 3 and 4). LHCSR has been reported to have a short fluorescence lifetime, particularly at low pH (Bonente et al., 2011), and could act by establishing pigment-pigment interactions with components of the PSII antenna system (either the reaction center or LHC components) to remove excess excitation energy and dissipate it as heat. LHCII, the only chlorophyll *b*-rich component (chlorophyll *a*/*b* = 1.4) in the stroma membranes (the PSI-LHCI complex being chlorophyll *a* enriched), appears to be directly quenched by LHCSR, based on the strong decrease of chlorophyll *b* contribution to PSI fluorescence upon quenching (Figures 6C and 6D). This is consistent with the reduced NPQ activity observed upon LhcbM1 depletion in *C. reinhardtii* (Elrad et al., 2002; Ferrante et al., 2012). Thus, although a stable LHCSR-PSI-LHCI-LHCII supercomplex could not be isolated under the experimental conditions used in this work, the results obtained from our functional measurements are strongly consistent with transient formation of such a pH-dependent/zeaxanthin-dependent complex.

Figure 6E summarizes our model of the relative contribution of LHCSR and PSBS to quenching events elicited by lumen acidification in *P. patens*. PSBS, mainly located in grana partitions where it interacts with the PSII antenna system (Teardo et al., 2007; Betterle et al., 2009), induces quenching in interacting LHCB proteins (Ahn et al., 2008). LHCSR, owing to its dual localization in grana margins and stroma-exposed membranes, can interact with components of the antenna system, most likely LHCII (Figures 6C and 6D), contributing to light harvesting by both photosystems (Figures 2G and 2H). It is interesting to discuss the reasons for the large LHCII complement to PSI antenna system and the need for its regulation by quenching in the moss. We note that PSI antenna moiety, LHCI, lacks a *Lhca4* ortholog in the *P. patens* genome and has low amplitude and not so red-shifted energy levels in mosses compared with higher plants, as shown by the 717-nm (versus 738-nm) fluorescence emission (Alboresi et al., 2008). The low amplitude of red-shifted spectral forms in the moss PSI together with the high LHCII complement in PSII antenna is likely to reduce the exciton supply to PSI in limiting light conditions due to competition by the spectrally overlapping PSII antenna system, leading to PQ overreduction. Interestingly, *C. reinhardtii*, also harboring a PSI-LHCI complex with a low content of red forms, has a large LHCI complex with nine subunits, versus four in plants (Bassi et al., 1992), which compensates for absorption by LHCII.

We suggest that LHCII fulfills a similar function in mosses, whose habitat is characterized by low light intensity interrupted by short HL sun flecks from clearings in the canopy. In these conditions, a constitutive enlargement of PSI antenna size by LHCII, coupled with the ability of rapid quenching in HL, appears to be the best option for optimal light use efficiency versus photoprotection balance. PSII is quenched first, followed by PSI, which, in turn, recovers its fluorescence faster in the dark (Figure 6B). This allows for preferential PSI activity over PSII during rapid changes in light intensity and moderates overreduction of the PQ pool and consequent photoinhibition (Vass et al., 1992; Finazzi et al., 2001). This effect is reminiscent of state 1 to state 2 transitions in higher plants and some green algae that prevent PQ overreduction by shuttling of a fraction of LHCII from PSII to PSI (Depège et al., 2003). Yet, in *P. patens*, excitation balance appears to be achieved by preferential quenching of the LHCII population that resides in grana membranes compared with that residing in stroma-exposed membranes.

METHODS

Plant Material and Growth Conditions

Physcomitrella patens subsp *patens* was grown in controlled-environment chambers with 16 h light (50 μmol photons m^{-2} s^{-1}) and 8 h dark at 24°C on rich $PpNH_4$ medium supplemented with 0.5% glucose as previously described (Ashton et al., 1979). Plants were propagated under sterile conditions on 9-cm Petri dishes overlaid with a cellophane disk (A.A. Packaging Limited), as previously described (Alboresi et al., 2008). For this study, the wild-type plants were used together with *psbs* KO, *lhcsr1* × *lhcsr2* KO (*lhcsr* KO), and *psbs x lhcsr1* × *lhcsr2 KO* (*npq4*) mutants (Alboresi et al., 2010). *Arabidopsis thaliana* plants were grown in a growth chamber for 6 weeks under controlled conditions (~120 μmol photons m^{-2} s^{-1}, 24°C, 8 h light/16 h dark, 70% relative humidity) and watered weekly with Coïc-Lesaint nutrient solution (Coïc and Lesaint, 1980).

NPQ Measurements at RT

In vivo chlorophyll fluorescence was measured at RT with a Dual PAM-100 fluorometer (Heinz Walz) using saturating light of 4000 μmol photons m^{-2} s^{-1} and actinic light of 850 μmol photons m^{-2} s^{-1} (HL). Measurements were made on protonemal tissue or functional chloroplasts (20 μg/mL chlorophyll) prepared according to Casazza et al. (2001). Fluorescence images in Figure 1A were obtained at RT with a FluorCam (Photon Systems Instruments).

Low-Temperature Fluorescence-Quenching Measurements

Functional chloroplasts, suspended at 20 μg/mL chlorophyll (Casazza et al., 2001), were added with 1 μM of recombinant GFP as an internal standard. Samples were illuminated with HL and frozen in liquid nitrogen still during illumination. As control, samples were frozen either before illumination or following a 5-min recovery in the dark. LT fluorescence was recorded using a Fluoromax3 equipped with an optical fiber (Horiba scientific). Emission spectra were performed by exciting the sample at 475 nm and recording emission in the 495- to 800-nm range. Chlorophyll emission spectra were normalized to the GFP signal at 513 nm. Excitation spectra were performed by recording emission at 717 nm for excitation in the 420- to 530-nm range. For quantitative analysis of PSI and PSII components of the spectra, a deconvolution was performed using four Gaussians peaking at 682, 693, 715, and 735 nm, respectively, which were attributed to LHCII (682), PSII core (693), and PSI-LHCI (715+735 nm) based on analysis of the individual complexes isolated from the sucrose gradient ultracentrifugation (Supplemental Figure 1). Elaboration of the spectra was performed using Origin 9.0 software (OriginLab). For each spectrum, the same maximum was initially kept fixed and the amplitudes and bandwidth changed to obtain a first approximate assembled spectrum. Subsequently, a fitting algorithm was run to obtain a more precise correlation.

SDS-PAGE and Immunoblot Analysis

SDS-PAGE analysis was performed as described (Laemmli, 1970) with minor modifications in order to separate LHCSR1 from LHCSR2 (Pinnola et al., 2013). Following electrophoresis, the gel was stained with Coomassie Brilliant Blue or proteins were transferred onto a polyvinylidene fluoride membrane (Millipore) using a Mini Trans-Blot cell (Bio-Rad) and detected by specific antibodies. α-*Hordeum vulgare* CP29 and PSBS (Bonente et al., 2008a), α-*P. patens* LHCSR1 protein (Pinnola et al., 2013), and α-Arabidopsis CP43 were homemade. α-PSAA (AS06 172) was

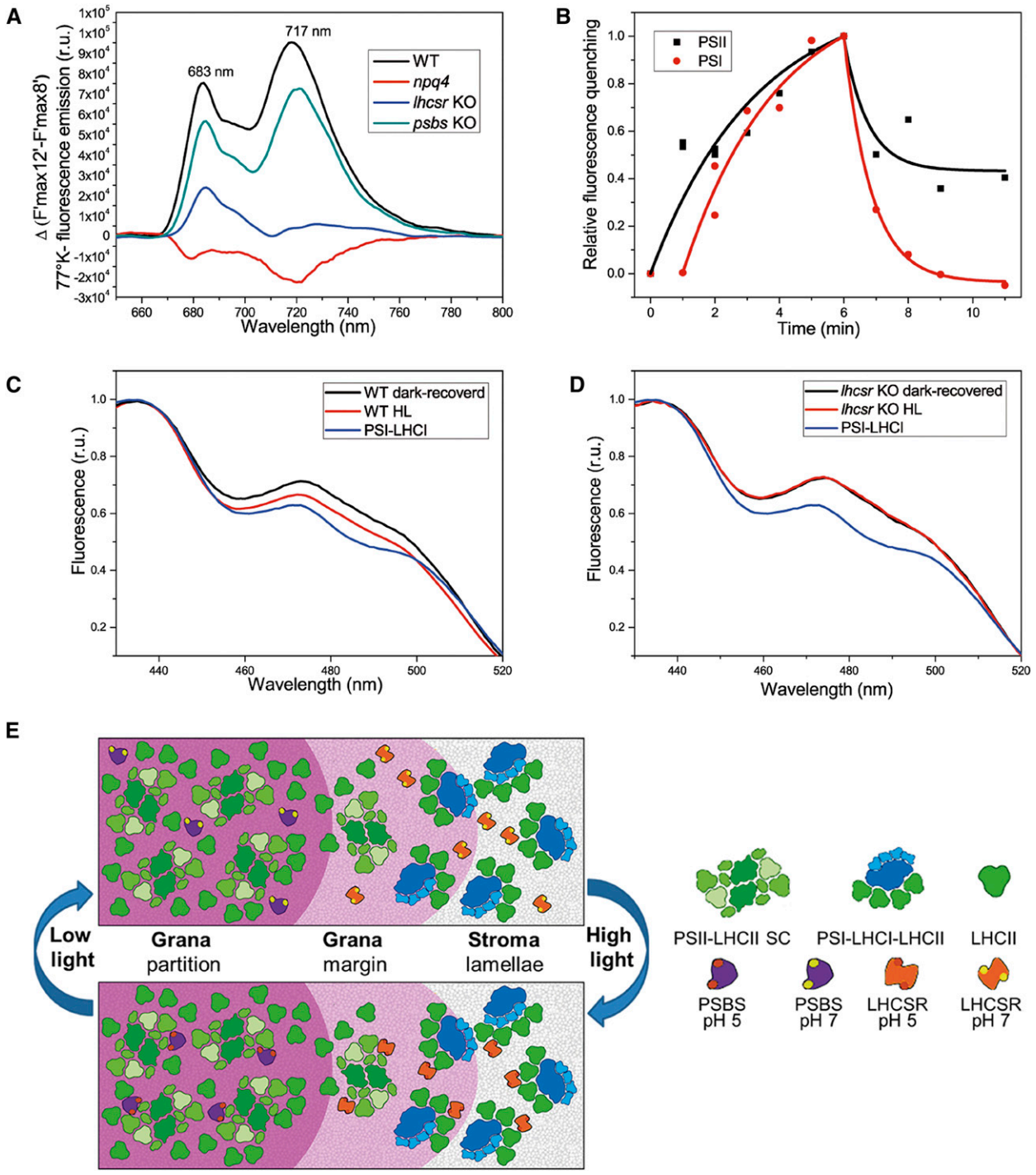

Figure 6. Changes in Chlorophyll *b* Contribution to PSI in 77K Fluorescence Excitation Spectra Depend on the Presence of LHCSR Proteins.

(A) Difference fluorescence emission spectra at 77K of dark recovery (5 min) minus HL treatment (6 min) using wild-type and mutant *P. patens* chloroplasts.
(B) Time course of the amplitude decrease of PSII (black squares) and PSI (red circles). Fluorescence emission components were deconvoluted from 77K spectra in wild-type chloroplasts that were illuminated at 850 µmol photons m^{-2} s^{-1} for 6 min and let recover in the dark for different times. A selection of the original spectra is shown in Figures 5E and 5F.
(C) and **(D)** The 77K fluorescence excitation spectra for PSI emission (717 nm) of 6 min HL (red) versus 5 min dark recovery (black) for the wild type **(C)** and *lhcsr* KO **(D)**. The spectrum using PSI-LHCI purified by sucrose gradient ultracentrifugation was included in both panels as a reference.
(E) Model for the LHCSR-dependent quenching of PSI and PSII fluorescence in *P. patens*: PSI fluorescence is decreased by quenching of LHCII antenna resident in the stroma lamellae and acting as antenna for PSI-LHCI complex. PSII fluorescence is decreased both by the action of the LHCSR fraction resident in the grana margins (from where it can interact with LHCII located both in grana and stroma membrane domains) and by the action of PSBS in the grana.

purchased by Agrisera. The signal amplitudes of the bands were quantified by GelPro 3.2 software (Bio-Rad).

Isolation and Fractionation of Thylakoid Membranes Using Digitonin

Stacked thylakoids were purified from protonemal tissue of *P. patens* plants following the same protocol used for seed plants (Bassi and Simpson, 1987). The solubilization protocol using digitonin was performed as described (Barbato et al., 2000; Sirpiö et al., 2007). Briefly, 0.4 mg chlorophyll/mL of thylakoids was incubated for 30 min in ice with stirring. Unsolubilized thylakoids were pelleted by centrifugation at 4000*g* for 5 min and granum-, margin-, and stroma-enriched fractions were isolated by centrifugation at 10,000*g* (10 min), 40,000*g* (30 min), and 100,000*g* (90 min), respectively.

Thylakoid Membrane Fractionation Using α-DM

Solubilization protocol using α-DM was performed as described (Morosinotto et al., 2010). Thylakoids (1 mg chlorophyll/mL) were solubilized at 4°C for 20 min in slow agitation with different amounts of α-DM ranging from 0.16 to 0.79% (w/v). Unsolubilized thylakoids were pelleted by centrifugation at 3500*g* for 5 min. Partially solubilized grana membranes were instead pelleted with a further 30-min centrifugation at 40,000*g*, whereas solubilized complexes and small membrane patches remained in the supernatant.

Mechanical Fractionation Using Yeda Press

Thylakoids were pellet by centrifugation, resuspended in 0.05 M HEPES-KOH, pH 7.5, 0.01 M $MgCl_2$, 0.001 M ascorbate, and 0.01 M NaF, and broken three times through a Yeda press at 120 bars (1 bar = 100 kPa). Stroma lamellae were purified by differential centrifugation as described by Bassi et al. (1988b).

Deriphat-PAGE

The different fractions (dmG and dmS) obtained solubilizing with α-DM were also analyzed by nondenaturing Deriphat-PAGE. This was performed following the method previously developed (Peter et al., 1991).

Analysis of P700 Redox State

Spectroscopic measurements were performed on thylakoids (20 μg/mL chlorophyll) or PSI-LHCI isolated from a sucrose gradient (6 μg/mL chlorophyll) using an LED spectrophotometer (JTS-10; Bio-Logic Science Instruments) in which absorption changes are sampled by weak monochromatic flashes (10-nm bandwidth) provided by LEDs. The relative antenna size of PSI was determined by analyzing time courses of P700 photooxidation upon illumination of the thylakoid suspension with weak far-red light (710 nm, 12 μmol photons m^{-2} s^{-1}). The reaction mixture contained 20 mM Tricine, pH 7.9, 10 mM NaCl, 5 mM $MgCl_2$, 50 μM 2,5-dibromo-3-methyl-6-isopropylbenzoquinone, and 1 mM methylviologen.

Immunogold Labeling and Electron Microscopy Analysis

Samples were fixed in 4% paraformaldehyde with 0.1% glutaraldehyde in 0.1 M cacodylate buffer (pH 7.4) for 1 h at room temperature and kept overnight at 4°C. The samples were soaked overnight in 2.3 M sucrose and rapidly frozen in liquid nitrogen. Frozen ultrathin (70 to 90 nm) sections were cut with a diamond knife at −120°C on a Leica EM UC6 ultramicrotome. The sections were collected on 200-mesh Formvar-coated nickel grids. Sections were blocked with a solution containing 1% BSA, 0.1% glycine, 0.1% gelatin, and 1% Tween 20. Immunolabeling was performed using affinity purified antibodies (α-LHCSR, α-PSBS, α-CP43, α-OEC, and α-LHCII) overnight at 4°C, followed by exposure to goat anti-rabbit IgG coupled to 10-nm gold particles (1:20; Jackson Immunoresearch) for 30 min at RT. Contrast staining and embedding were performed as previously described (Tokuyasu, 1986). The embedded sections were examined and imaged with an FEI Tecnai SPIRIT transmission electron microscope operating at 120 kV and equipped with an EAGLE CCD Camera. Gold granules were counted over well-defined stacked and unstacked membranes, the length of which was measured in order to obtain the du/ds value. du/ds is the ratio of labeled particles over unstacked(du)/stacked(ds) membranes and is deduced using the following formula:

$$\delta = \frac{1}{1 + \frac{\sigma}{du/ds*(1-\sigma)}}$$

in which δ is the percentage of labeled particles found in the unstacked region and σ is the percentage of stacked membranes measured on the same images (Vallon et al., 1991).

Accession Numbers

Sequence data from this article can be found in the GenBank/EMBL data libraries under the following accession numbers: DS545130 (Pp1s241_86V6, PSBS), DS545102 (Pp1s213_80V6, LHCSR1), and DS544988 (Pp1s99_95V6, LHCSR2).

Supplemental Data

Supplemental Figure 1. Sucrose gradient fractionation of thylakoids from *P. patens* (*P.p.*) and *A. thaliana* (*A.t.*).

Supplemental Figure 2. Immunoblot analysis of *P. patens* thylakoid membrane fractions from digitonin and Yeda press treatments.

Supplemental Figure 3. Analysis of fractions from *P. patens* thylakoids upon titration with a range of α-DM concentrations.

Supplemental Figure 4. Immunodetection of PSBS and LHCSR, PSAA, and CP43 in fractions from α-DM-treated thylakoids.

Supplemental Figure 5. Distribution of PSI and PSII upon exposure for 10 min to either CL (50 μmol photons m^{-2} s^{-1}) or HL (850 μmol photons m^{-2} s^{-1}).

Supplemental Figure 6. 77K fluorescence emission spectra of *P. patens* intact chloroplasts in quenched state (black) or upon recovery in the dark (gray).

AUTHOR CONTRIBUTIONS

A.P. carried out the growth and characterization of *P. patens* genotypes, the NPQ measurements, the fractionation of thylakoids, and the biochemical characterization of the different fractions with the initial contribution of A.A. S.C. was involved in LT fluorescence spectroscopy and electron microscopy data analysis. R.N., S.L.-Z., and Z.R. carried out the immunoelectron microscopy. R.B. conceived the study, participated in its design and coordination, performed the negative staining electron microscopy, and wrote the article.

ACKNOWLEDGMENTS

Research was funded in part through the European Union Seventh Framework Programme for Research Project 316427, Environmental Acclimation of Photosynthesis, and the Italian Ministry of Agriculture, Food, and Forestry Project HYDROBIO. The immunoelectron microscopy studies were conducted at the Irving and Cherna Moskowitz Center for Nano and Bio-Nano Imaging at the Weizmann Institute of Science (WIS). Work performed at the WIS was funded by grants (to Z.R.) from the Israel Science

Foundation (No. 1034/12), Human Frontier Science Program (RGP0005/2013), and Carolito Stiftüng.

Received May 18, 2015; revised September 15, 2015; accepted October 7, 2015; published October 27, 2015.

REFERENCES

Ahn, T.K., Avenson, T.J., Ballottari, M., Cheng, Y.-C., Niyogi, K.K., Bassi, R., and Fleming, G.R. (2008). Architecture of a charge-transfer state regulating light harvesting in a plant antenna protein. Science **320:** 794–797.

Alboresi, A., Caffarri, S., Nogue, F., Bassi, R., and Morosinotto, T. (2008). In silico and biochemical analysis of *Physcomitrella patens* photosynthetic antenna: identification of subunits which evolved upon land adaptation. PLoS One **3:** e2033.

Alboresi, A., Gerotto, C., Giacometti, G.M., Bassi, R., and Morosinotto, T. (2010). *Physcomitrella patens* mutants affected on heat dissipation clarify the evolution of photoprotection mechanisms upon land colonization. Proc. Natl. Acad. Sci. USA **107:** 11128–11133.

Andersson, B., and Anderson, J.M. (1980). Lateral heterogeneity in the distribution of chlorophyll-protein complexes of the thylakoid membranes of spinach chloroplasts. Biochim. Biophys. Acta **593:** 427–440.

Ashton, N.W., Grimsley, N.H., and Cove, D.J. (1979). Analysis of gametophytic development in the moss, *Physcomitrella patens*, using auxin and cytokinin resistant mutants. Planta **144:** 427–435.

Ballottari, M., Mozzo, M., Girardon, J., Hienerwadel, R., and Bassi, R. (2013). Chlorophyll triplet quenching and photoprotection in the higher plant monomeric antenna protein Lhcb5. J. Phys. Chem. B **117:** 11337–11348.

Barbato, R., Bergo, E., Szabò, I., Dalla Vecchia, F., and Giacometti, G.M. (2000). Ultraviolet B exposure of whole leaves of barley affects structure and functional organization of photosystem II. J. Biol. Chem. **275:** 10976–10982.

Baroli, I., Do, A.D., Yamane, T., and Niyogi, K.K. (2003). Zeaxanthin accumulation in the absence of a functional xanthophyll cycle protects *Chlamydomonas reinhardtii* from photooxidative stress. Plant Cell **15:** 992–1008.

Bassi, R., Giacometti, G., and Simpson, D.J. (1988a). Characterisation of stroma membranes from *Zea mays* L. chloroplasts. Carlsberg Res. Commun. **53:** 221–232.

Bassi, R., Giacometti, G.M., and Simpson, D. (1988b). Changes in the composition of stroma lamellae following state I-state II transitions. Biochim. Biophys. Acta **935:** 152–165.

Bassi, R., Soen, S.Y., Frank, G., Zuber, H., and Rochaix, J.D. (1992). Characterization of chlorophyll a/b proteins of photosystem I from *Chlamydomonas reinhardtii*. J. Biol. Chem. **267:** 25714–25721.

Bassi, R., and Simpson, D. (1987). Chlorophyll-protein complexes of barley photosystem I. Eur. J. Biochem. **163:** 221–230.

Ben-Shem, A., Frolow, F., and Nelson, N. (2003). Crystal structure of plant photosystem I. Nature **426:** 630–635.

Bergner, S.V., Scholz, M., Trompelt, K., Barth, J., Gäbelein, P., Steinbeck, J., Xue, H., Clowez, S., Fucile, G., Goldschmidt-Clermont, M., Fufezan, C., and Hippler, M. (2015). STATE TRANSITION7-dependent phosphorylation is modulated by changing environmental conditions and its absence triggers remodeling of photosynthetic protein complexes. Plant Physiol. **168:** 615–634

Betterle, N., Ballottari, M., Zorzan, S., de Bianchi, S., Cazzaniga, S., Dall'osto, L., Morosinotto, T., and Bassi, R. (2009). Light-induced dissociation of an antenna hetero-oligomer is needed for non-photochemical quenching induction. J. Biol. Chem. **284:** 15255–15266.

Bonente, G., Ballottari, M., Truong, T.B., Morosinotto, T., Ahn, T.K., Fleming, G.R., Niyogi, K.K., and Bassi, R. (2011). Analysis of LhcSR3, a protein essential for feedback de-excitation in the green alga *Chlamydomonas reinhardtii*. PLoS Biol. **9:** e1000577.

Bonente, G., Howes, B.D., Caffarri, S., Smulevich, G., and Bassi, R. (2008a). Interactions between the photosystem II subunit PsbS and xanthophylls studied in vivo and in vitro. J. Biol. Chem. **283:** 8434–8445.

Bonente, G., Passarini, F., Cazzaniga, S., Mancone, C., Buia, M.C., Tripodi, M., Bassi, R., and Caffarri, S. (2008b). The occurrence of the psbS gene product in *Chlamydomonas reinhardtii* and in other photosynthetic organisms and its correlation with energy quenching. Photochem. Photobiol. **84:** 1359–1370.

Busch, A., Petersen, J., Webber-Birungi, M.T., Powikrowska, M., Lassen, L.M.M., Naumann-Busch, B., Nielsen, A.Z., Ye, J., Boekema, E.J., Jensen, O.N., Lunde, C., and Jensen, P.E. (2013). Composition and structure of photosystem I in the moss *Physcomitrella patens*. J. Exp. Bot. **64:** 2689–2699.

Cardol, P., Forti, G., and Finazzi, G. (2011). Regulation of electron transport in microalgae. Biochim. Biophys. Acta **1807:** 912–918.

Casazza, A.P., Tarantino, D., and Soave, C. (2001). Preparation and functional characterization of thylakoids from *Arabidopsis thaliana*. Photosynth. Res. **68:** 175–180.

Cho, F., Spencer, J., and Govindjee. (1966). Emission spectra of Chlorella at very low temperatures (-269 degrees to -196 degrees). Biochim. Biophys. Acta **126:** 174–176.

Coïc, Y., and Lesaint, C. (1980). [Determination of the accumulation of nitrates in plant tissues]. Ann. Nutr. Aliment. **34:** 929–936.

Dainese, P., and Bassi, R. (1991). Subunit stoichiometry of the chloroplast photosystem II antenna system and aggregation state of the component chlorophyll a/b binding proteins. J. Biol. Chem. **266:** 8136–8142.

Dall'Osto, L., Caffarri, S., and Bassi, R. (2005). A mechanism of nonphotochemical energy dissipation, independent from PsbS, revealed by a conformational change in the antenna protein CP26. Plant Cell **17:** 1217–1232.

Dall'Osto, L., Cazzaniga, S., Havaux, M., and Bassi, R. (2010). Enhanced photoprotection by protein-bound vs free xanthophyll pools: a comparative analysis of chlorophyll b and xanthophyll biosynthesis mutants. Mol. Plant **3:** 576–593.

Dall'Osto, L., Holt, N.E., Kaligotla, S., Fuciman, M., Cazzaniga, S., Carbonera, D., Frank, H.A., Alric, J., and Bassi, R. (2012). Zeaxanthin protects plant photosynthesis by modulating chlorophyll triplet yield in specific light-harvesting antenna subunits. J. Biol. Chem. **287:** 41820–41834.

de Bianchi, S., Ballottari, M., Dall'osto, L., and Bassi, R. (2010). Regulation of plant light harvesting by thermal dissipation of excess energy. Biochem. Soc. Trans. **38:** 651–660.

Depège, N., Bellafiore, S., and Rochaix, J.-D. (2003). Role of chloroplast protein kinase Stt7 in LHCII phosphorylation and state transition in Chlamydomonas. Science **299:** 1572–1575.

Dominici, P., Caffarri, S., Armenante, F., Ceoldo, S., Crimi, M., and Bassi, R. (2002). Biochemical properties of the PsbS subunit of photosystem II either purified from chloroplast or recombinant. J. Biol. Chem. **277:** 22750–22758.

Elrad, D., Niyogi, K.K., and Grossman, A.R. (2002). A major light-harvesting polypeptide of photosystem II functions in thermal dissipation. Plant Cell **14:** 1801–1816.

Ferrante, P., Ballottari, M., Bonente, G., Giuliano, G., and Bassi, R. (2012). LHCBM1 and LHCBM2/7 polypeptides, components of major LHCII complex, have distinct functional roles in photosynthetic antenna system of *Chlamydomonas reinhardtii*. J. Biol. Chem. **287:** 16276–16288.

Finazzi, G., Zito, F., Barbagallo, R.P., and Wollman, F.A. (2001). Contrasted effects of inhibitors of cytochrome b6f complex on state transitions in *Chlamydomonas reinhardtii*: the role of Qo site occupancy in LHCII kinase activation. J. Biol. Chem. **276:** 9770–9774.

Funk, C., Schröder, W.P., Green, B.R., Renger, G., and Andersson, B. (1994). The intrinsic 22 kDa protein is a chlorophyll-binding subunit of photosystem II. FEBS Lett. **342:** 261–266.

Harrer, R., Bassi, R., Testi, M.G., and Schäfer, C. (1998). Nearest-neighbor analysis of a photosystem II complex from *Marchantia polymorpha* L. (liverwort), which contains reaction center and antenna proteins. Eur. J. Biochem. **255:** 196–205.

Johnson, M.P., Goral, T.K., Duffy, C.D.P., Brain, A.P.R., Mullineaux, C.W., and Ruban, A.V. (2011). Photoprotective energy dissipation involves the reorganization of photosystem II light-harvesting complexes in the grana membranes of spinach chloroplasts. Plant Cell **23:** 1468–1479.

Kalituho, L., Beran, K.C., and Jahns, P. (2007). The transiently generated nonphotochemical quenching of excitation energy in Arabidopsis leaves is modulated by zeaxanthin. Plant Physiol. **143:** 1861–1870.

Krause, G.H., Briantais, J.-M., and Vernotte, C. (1983). Characterization of chlorophyll fluorescence quenching in chloroplasts by fluorescence spectroscopy at 77 K I. ΔpH-dependent quenching. Biochim. Biophys. Acta **723:** 169–175.

Laemmli, U.K. (1970). Cleavage of structural proteins during the assembly of the head of bacteriophage T4. Nature **227:** 680–685.

Li, X.P., Björkman, O., Shih, C., Grossman, A.R., Rosenquist, M., Jansson, S., and Niyogi, K.K. (2000). A pigment-binding protein essential for regulation of photosynthetic light harvesting. Nature **403:** 391–395.

Liguori, N., Roy, L.M., Opacic, M., Durand, G., and Croce, R. (2013). Regulation of light harvesting in the green alga *Chlamydomonas reinhardtii*: the C-terminus of LHCSR is the knob of a dimmer switch. J. Am. Chem. Soc. **135:** 18339–18342.

Liu, Z., Yan, H., Wang, K., Kuang, T., Zhang, J., Gui, L., An, X., and Chang, W. (2004). Crystal structure of spinach major light-harvesting complex at 2.72 A resolution. Nature **428:** 287–292.

Mazor, Y., Borovikova, A., and Nelson, N. (2015). The structure of plant photosystem I super-complex at 2.8 Å resolution. eLife **4:** e07433.

Morosinotto, T., Segalla, A., Giacometti, G.M., and Bassi, R. (2010). Purification of structurally intact grana from plants thylakoids membranes. J. Bioenerg. Biomembr. **42:** 37–45.

Nevo, R., Charuvi, D., Tsabari, O., and Reich, Z. (2012). Composition, architecture and dynamics of the photosynthetic apparatus in higher plants. Plant J. **70:** 157–176.

Niyogi, K.K., and Truong, T.B. (2013). Evolution of flexible non-photochemical quenching mechanisms that regulate light harvesting in oxygenic photosynthesis. Curr. Opin. Plant Biol. **16:** 307–314.

Peers, G., Truong, T.B., Ostendorf, E., Busch, A., Elrad, D., Grossman, A.R., Hippler, M., and Niyogi, K.K. (2009). An ancient light-harvesting protein is critical for the regulation of algal photosynthesis. Nature **462:** 518–521.

Peter, G.F., Takeuchi, T., and Philip Thornber, J. (1991). Solubilization and two-dimensional electrophoretic procedures for studying the organization and composition of photosynthetic membrane polypeptides. Methods **3:** 115–124.

Pinnola, A., Dall'Osto, L., Gerotto, C., Morosinotto, T., Bassi, R., and Alboresi, A. (2013). Zeaxanthin binds to light-harvesting complex stress-related protein to enhance nonphotochemical quenching in *Physcomitrella patens*. Plant Cell **25:** 3519–3534.

Rensing, S.A., et al. (2008). The Physcomitrella genome reveals evolutionary insights into the conquest of land by plants. Science **319:** 64–69.

Simpson, D.J. (1983). Freeze-fracture studies on barley plastid membranes. VI. Location of the P700-chlorophyll a-protein 1. Eur. J. Cell Biol. **31:** 305–314.

Sirpiö, S., Allahverdiyeva, Y., Suorsa, M., Paakkarinen, V., Vainonen, J., Battchikova, N., and Aro, E.-M. (2007). TLP18.3, a novel thylakoid lumen protein regulating photosystem II repair cycle. Biochem. J. **406:** 415–425.

Teardo, E., de Laureto, P.P., Bergantino, E., Dalla Vecchia, F., Rigoni, F., Szabò, I., and Giacometti, G.M. (2007). Evidences for interaction of PsbS with photosynthetic complexes in maize thylakoids. Biochim. Biophys. Acta **1767:** 703–711.

Tikkanen, M., Suorsa, M., Gollan, P.J., and Aro, E.-M. (2012). Post-genomic insight into thylakoid membrane lateral heterogeneity and redox balance. FEBS Lett. **586:** 2911–2916.

Tokutsu, R., and Minagawa, J. (2013). Energy-dissipative supercomplex of photosystem II associated with LHCSR3 in *Chlamydomonas reinhardtii*. Proc. Natl. Acad. Sci. USA **110:** 10016–10021.

Tokuyasu, K.T. (1986). Application of cryoultramicrotomy to immunocytochemistry. J. Microsc. **143:** 139–149.

Vallon, O., Bulte, L., Dainese, P., Olive, J., Bassi, R., and Wollman, F.A. (1991). Lateral redistribution of cytochrome b6/f complexes along thylakoid membranes upon state transitions. Proc. Natl. Acad. Sci. USA **88:** 8262–8266.

Vass, I., Styring, S., Hundal, T., Koivuniemi, A., Aro, E., and Andersson, B. (1992). Reversible and irreversible intermediates during photoinhibition of photosystem II: stable reduced QA species promote chlorophyll triplet formation. Proc. Natl. Acad. Sci. USA **89:** 1408–1412.

Xue, H., Tokutsu, R., Bergner, S.V., Scholz, M., Minagawa, J., and Hippler, M. (2015). PHOTOSYSTEM II SUBUNIT R is required for efficient binding of LIGHT-HARVESTING COMPLEX STRESS-RELATED PROTEIN3 to photosystem II-light-harvesting supercomplexes in *Chlamydomonas reinhardtii*. Plant Physiol. **167:** 1566–1578.

Light-Harvesting Complex Stress-Related Proteins Catalyze Excess Energy Dissipation in Both Photosystems of *Physcomitrella patens*

Alberta Pinnola, Stefano Cazzaniga, Alessandro Alboresi, Reinat Nevo, Smadar Levin-Zaidman, Ziv Reich and Roberto Bassi

Plant Cell 2015;27;3213-3227; originally published online October 27, 2015;
DOI 10.1105/tpc.15.00443